Theses and Dissertations

2012-08-09

Curious Growth of a Buried SiO2 Layer

Thomas O. McConkie
Brigham Young University - Provo

Follow this and additional works at: https://scholarsarchive.byu.edu/etd

Part of the Astrophysics and Astronomy Commons, and the Physics Commons

BYU ScholarsArchive Citation

Curious Growth of a Buried SiO$_2$ Layer

Thomas O. McConkie

A thesis submitted to the faculty of
Brigham Young University
in partial fulfillment of the requirements for the degree of

Master of Science

Richard Vanfleet, Chair
Branton Campbell
Robert Davis

Department of Physics and Astronomy

Brigham Young University

December 2012

ABSTRACT

Curious Growth of a Buried SiO_2 Layer

Thomas O. McConkie
Department of Physics and Astronomy, BYU
Master of Science

Initial investigation of Moxtek wire grid polarizers composed of Al and coated with SiO_2 - SiX - SiO_2 (where SiX is used to indicate a Si rich layer whose complete composition is not to be disclosed for proprietary reasons) showed a growth of 3x in the inner (closest to Al) SiO_2 layer after baking. Upon removing the X and varying rib composition and layering composition and geometries in 12 sets of before and after samples, no obvious growth was observed. Even baking the original unbaked sample yielded no growth. Our data suggest that the initial conclusion of buried oxide growth was flawed and that the observed changes in optical properties upon baking are either very sensitive to layer thicknesses (smaller than we can confidently observe) or due to some other mechanism. Here we present our sample preparation and analysis using the Focused Ion Beam (FIB), Scanning Transmission Electron Microscopy (STEM), and Energy Dispersive Xray Spectroscopy (EDXS).

ACKNOWLEDGMENTS

Contents

Chapter 1

Introduction

Silicon dioxide has become an essential part of the semiconductor industry. As such there have been copious amounts of research done on this compound. However, even with its popularity among researchers over the past 50 plus years the mechanism of oxidation remains a great debate. The model most widely accepted was proposed by B. E. Deal and A. S. Grove of Fairchild Semiconductor in 1965 (Deal & Grove 1965). The Deal-Grove model assumes that the oxidation takes place at the boundary between the SiO_2 layer and the bulk silicon. This is to say that the gaseous O_2 diffuses through the SiO_2 layer and then reacts with the bulk silicon at the boundary. Recently Angelo Bongiorno and Alfredo Pasquarello affirmed that this was the case in 2002 through their Monte Carlo first-principles simulation (Bongiorno & Pasquarello 2002).

However, not everyone is in agreement with this model. Akermark in 2000 published a paper stating that atomic oxygen is a more likely candidate for the transported species (Akermark 2000). In support of Akermark, Zhong et al. published a paper stating that "the diffusion mechanism in SiO_2 during water vapor oxidation is exchange diffusion "(Zhong et al. 2009). Exchange diffusion is the notion that the SiO_2 at the air-oxide interface reacts with the O_2 in the air by accepting extra O atoms. These oxygen rich molecules then release their excess O into the oxide layer, which in turn attach to another SiO_2 molecule prompting a cascading effect of O migration toward the

1

Si-SiO$_2$ interface. Upon reaching the interface the O then oxidizes Si atoms from the bulk.

There do exist some parties that are taking the middle ground on this issue. Hamann identified "the peroxy linkage as the lowest energy configuration of atomic O in SiO$_2$, and [found] that its energy in this site and in interstitial molecular O$_2$ are nearly equal;" therefore, both mechanisms may contribute (Hamann 1998). Also Gusev et al. in 1995 state that the Deal-Grove model appears to only apply for oxides greater than 40 Å(Gusev et al. 1995). On the other hand, Liu et al. found the lower limit to be 8 nm (Lu et al. 1995).

Another phenomenon in silicon oxidation found in the literature is that of differing oxidation rates due to curvature. Kao et al in 1987 showed experimentally using cylindrical silicon structures that "oxidation of curved silicon surfaces is retarded at low temperatures and sharp curvatures and that the retardation is more severe on concave than convex structures" (Kao et al. 1987).

1.1 Problem

The company Moxtek is a world producer of high intensity polarizers. In an effort to improve their product they have coated the polarizing ribs with a multilayer structure. They found that after baking at 300°C for >100 hrs (simulating long term use) the transmission and reflection curves shifted in frequency. I was asked to analyze these polarizers and look for evidence of a physical change that would cause this phenomenon. These polarizers are constructed of a glass substrate supporting an array of aluminum ribs running the length of the glass (Figure 1.1). As mentioned before each of these ribs is coated with thin films (SiO$_2$, SiX) in an effort to make the polarizers more robust to high intensity light. The ribs are spaced $\sim$ 100 nm apart. The match head (top of the rib) consists of layered SiO$_2$, Si and SiO$_2$, measuring about 10nm, 15nm, 10 nm respectively parallel to the rib. The widest horizontal measurement (perpendicular to the rib) of the match head is $\sim$ 60 nm. I was given before and after baking sample sets for comparison. In one case the

aluminum ribs were coated first with SiO_2, then a Si rich SiX layer, and finally SiO_2 again. In order to protect proprietary information the term SiX is used to indicate a Si rich layer whose complete composition is not to be disclosed. It was found that after baking, the inner SiO_2 layer was much thicker than that of the unbaked sample. Figure 1.2 shows these unbaked and baked samples. It is recognized that there is a visual difference between the two samples. These samples either, started out with different Al rib geometries then coated by the same process making them comparable or are two different samples and therefore incomparable. The evidence of this supposed growth is given in this section.

Figure 1.3 shows the elemental profile of the unbaked sample. This profile is what we see from a scan directly up and down from the aluminum rib through the coating (the process of acquiring this data is described in section 3.2). The blue, red, and yellow profiles in the figure represent the Al, Si and O counts respectively. The two profiles shown are the trace and retrace of roughly the same path. Region of Interest I (ROI I) points out that the Al profiles are in good agreement. This agreement allows us to have confidence in the spatial comparison of the Si and O profiles.

ROI II highlights the good spatial agreement in the location of our Si and O. It also shows the SiO_2 layer covering the Al, followed by a region of Si and then another SiO_2 layer. The SiO_2 layer is indicated by the matching rise and subsequent diverging slopes of the Si and O profiles. The Si layer is indicated by the high Si count and low O count. The final SiO_2 layer is again indicated by the rise in the O counts and subsequent decrease of the O and Si counts. ROI III highlights a mismatch of the O counts in the first O peak. This mismatch and that of the Si profile widths in ROI II are most likely a result of the trace and re-trace not following exactly the same path.

Figure 1.4 shows the elemental profile of the sample after being baked at 300^oC for 168 hrs. There are clear differences between this profile and that in Figure 1.3 (the unbaked profile). ROI I shows the relative agreement of the O and Si profiles. Also in this region we note the relative difference in height and width of the first (closest to the Al) O peak to that of the second. These
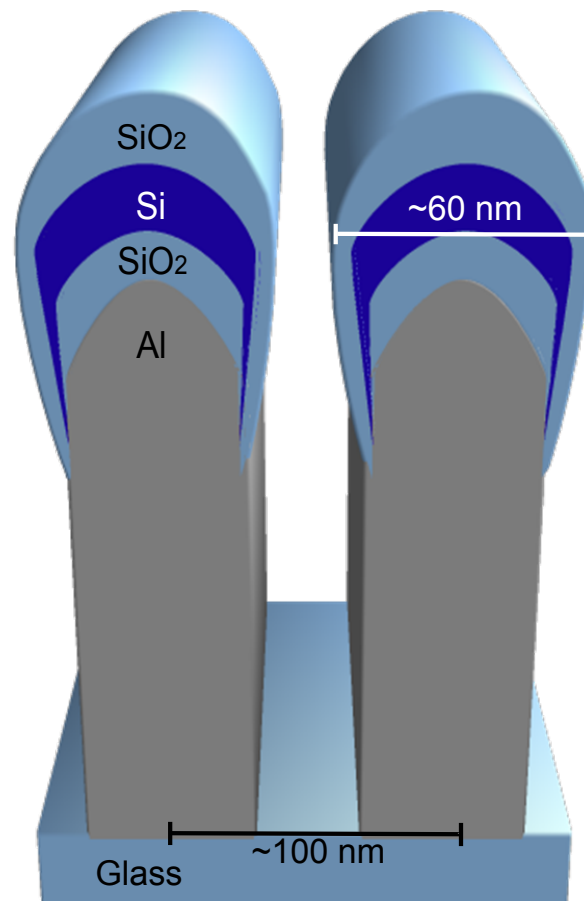
Figure 1.1 Here is a general graphic of the rib anatomy (not to scale). The polarizers are composed of aluminum ribs coated with SiO_2 , Si and SiO_2 on a glass substrate.The ribs are spaced ~ 100 nm on center. The match head (top of the rib) consists of layered SiO_2 , Si and SiO_2 measuring about 10nm, 15nm, 10 nm respectively parallel to the rib. The widest horizontal measurement (perpendicular to the rib) of the match head is ~ 60 nm.
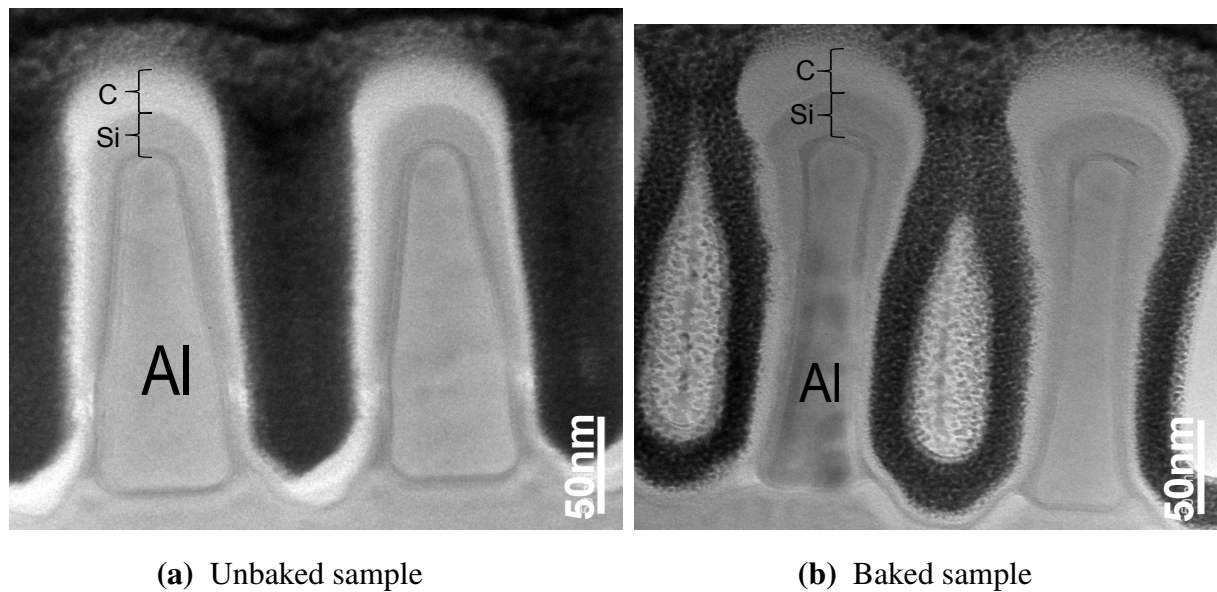
(a) Unbaked sample   **(b)** Baked sample

Figure 1.2 (a) Mass thickness contrast image of the unbaked sample. (b) Mass thickness contrast image of the baked sample. As labeled, the ribs are composed of Al, coated with the Si layers and also coated with C. Note the different shapes of the Al ribs. This difference indicates the suspicion that they may not be comparable but if the deposition process of the Si layers was the same for then they should be comparable.
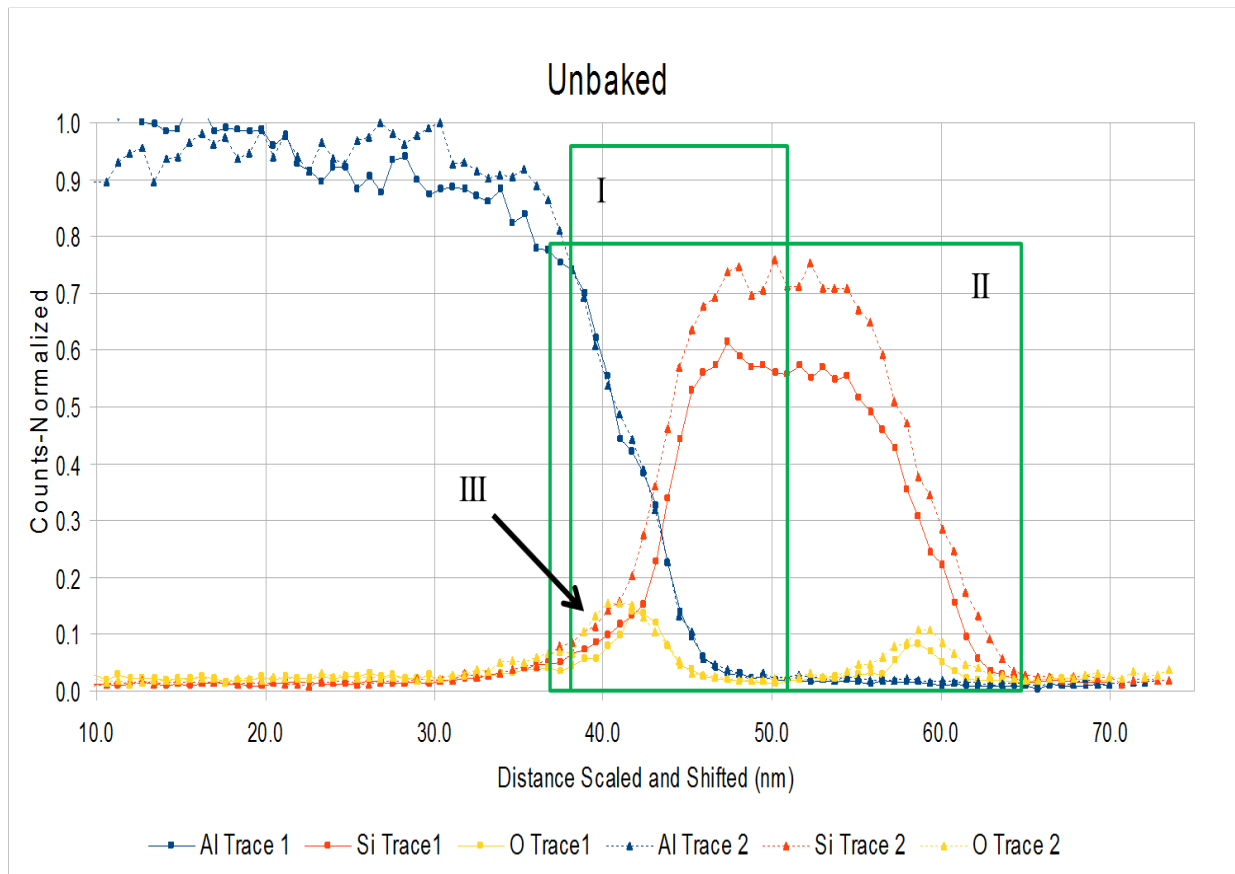
Figure 1.3 This is data is from a scan directly up and down from the aluminum rib through the Si coating of the unbaked sample. It is against this profile that we will compare the baked profile. I highlights the alignment of the Al shoulder. II shows the alternating SiO_2, Si, SiO_2 layers. III highlights a slight discrepancy in the oxygen profiles.
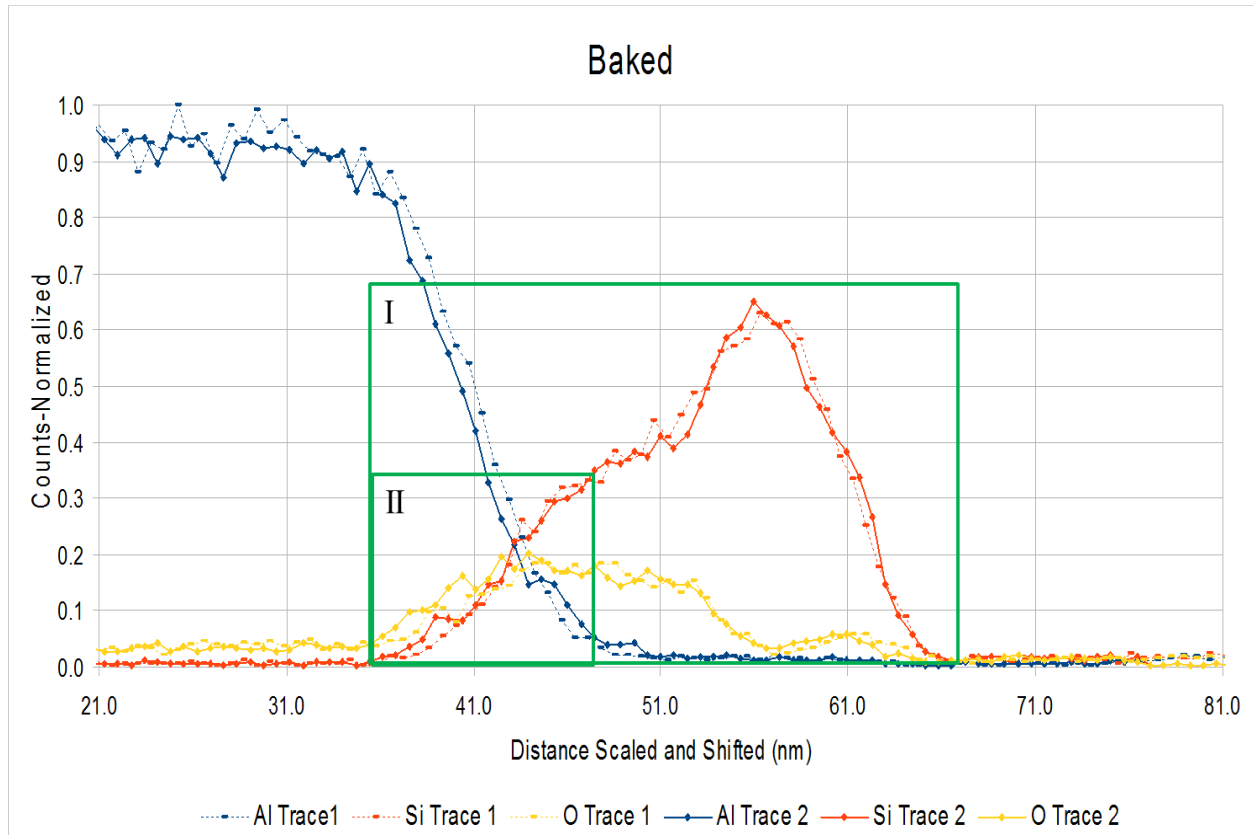
Figure 1.4 This profile is from a baked sample. It is in this profile that we see the thicker SiO_2 layer covering the Al. I is pointing out the good agreement of the Si and O trace and retrace. II points out a difference of the O profiles.

features indicate a thick SiO_2 layer, followed by a Si layer capped with a thin SiO_2 layer. This differs from what we saw in the unbaked case. ROI II highlights a slight difference in O counts in the trace and re-trace.

In Figure 1.5 the baked and unbaked profiles have been overlaid. For this comparison the aluminum profiles were aligned, assuming that they were undisturbed during the baking process. In ROI I it is shown that the first O peak of the baked sample is much larger than that of the

unbaked. It is also shown that the shape of the Si profiles are different between the two samples. The final difference to point out in this region is that of the outer O peaks; the unbaked peak is larger and closer to the Al than the corresponding baked O peak. The difference in the first O peak profiles and the corresponding shoulder in the Si counts indicates a thicker SiO_2 layer. The lack of the top plateau in the baked sample as seen in the unbaked sample is due to a thinner SiX region. The shift in the outer baked O peak must be due to the growth of the inner SiO_2 layer since SiO_2 is less dense.

Fig 1.6 is a rescaling of figure 1.5. In order to allow a closer inspection of the O profiles, the Al and Si profiles have been removed. Here we can more clearly see that not only is the inner O peak of the baked sample wider than that of the unbaked sample, but also the baked outside O peak is further away from the Al than the unbaked outside O peak as was mentioned earlier. This suggests a degree of physical growth. It is expected that the outside O peaks would experience a smaller shift than the inner peaks since radial growth is assumed. It is interesting to note that the Si counts on that side do not show as large of a shift as the O peaks.

The expansion of the inner O peak, the corresponding shoulder in the Si profile, and the shift in the outer O peaks, indicates that the innermost layer of SiO_2 is growing during the baking process. Oxygen is selectively oxidizing the inner silicon at the Si-SiO_2 boundary. In this manuscript we attempt to address the questions of how the O arrives at the site and why the inner layer has grown but the outer layer shows no such growth.

Here are a few hypotheses to explain the arrival of the O.

- Excess oxygen in the inner oxide layer. Perhaps the inner oxide layer may be non-stoichiometric and may contain more oxygen than needed. When heated, the excess O migrates out to oxidize the Si capping layer. This would then cause an increase in the SiO_2 layer width.

- Free oxygen in the aluminum. Similar to the above hypothesis, but the O needed to oxidize the Si rich layer would originate in the Al rib and diffuse out of the Al and through the SiO_2
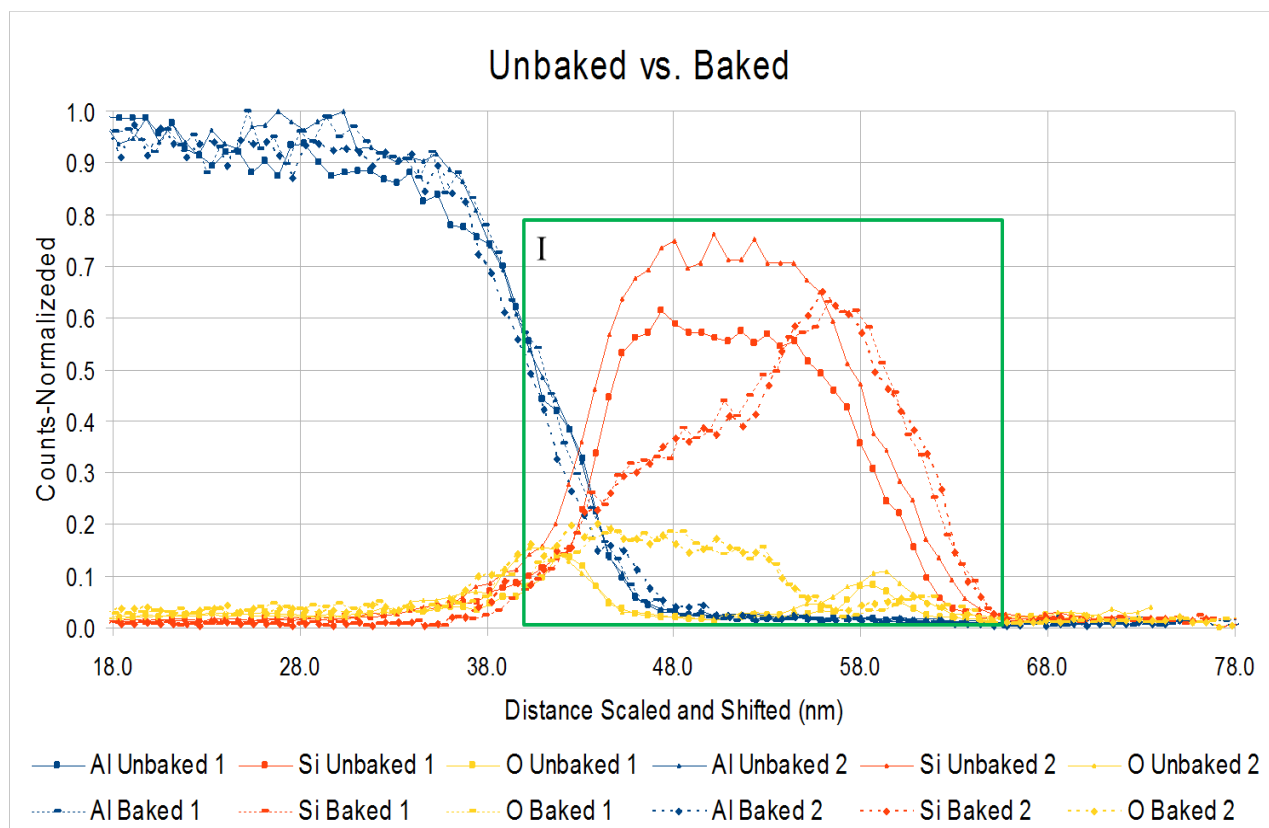
Figure 1.5 This is the comparison of both the baked (Fig 1.4) and unbaked (Fig 1.3) profiles. The Al shoulder has been aligned thus allowing us to compare the horizontal position of the O and Si profiles. I is calling attention to the main region of differences between the baked and unbaked profiles discussed in the text.
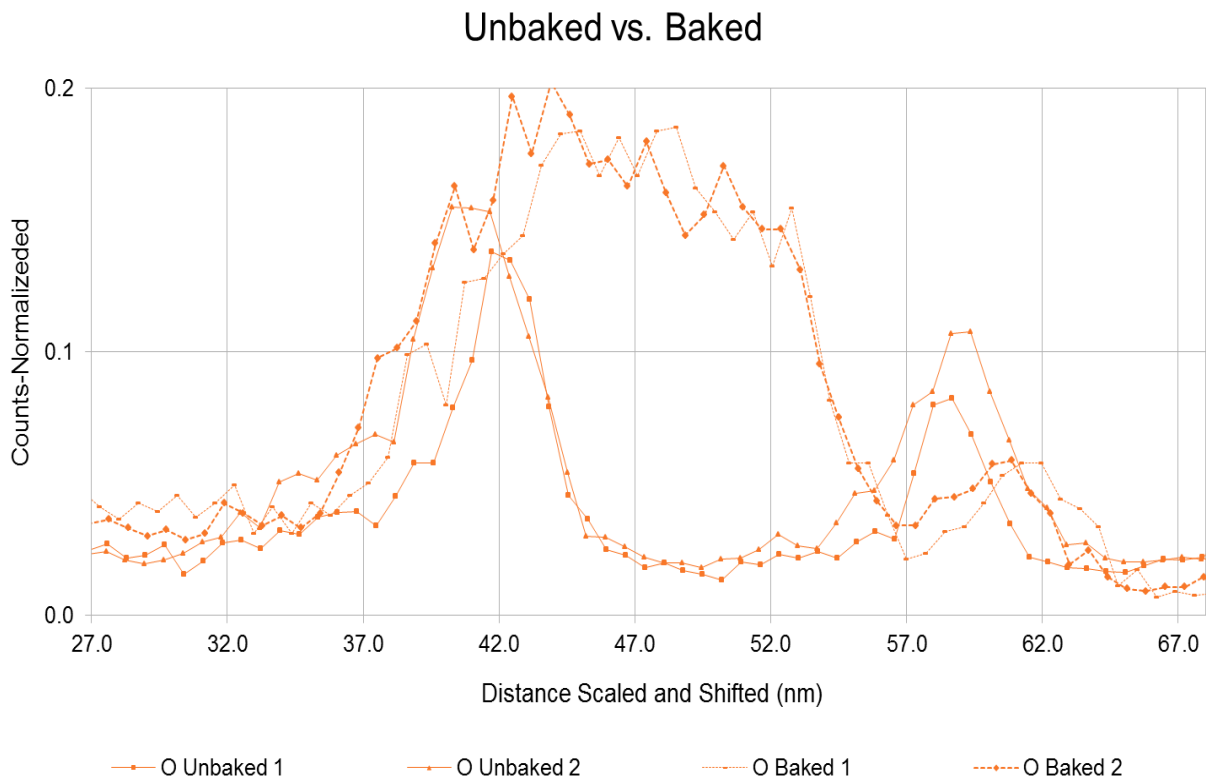
Unbaked vs. Baked

Figure 1.6 This graph highlights the O profiles of figure 1.5. Here it is easier to see the O growth that was observed.

layer during the baking process.

- O migration up the Si-SiO_2 or Al-SiO_2 interface or SiO_2 itself. This hypothesis speculates that the O originates in the atmosphere and wicks up the Si-SiO_2 or Al-SiO_2 interface or through the SiO_2 itself entering at the side of the rib.

- Atmospheric O diffusing through the SiO_2 and Si rich layers.

Here are a few hypotheses to explain the preferential oxidation of the inner layer.

- Al_2O_3 catalysis. A thin film of alumina on the surface of the rib is acting as a catalysis for this oxidation. Recognizing that the oxidation of Si is a slow process this catalysis could account of the greater growth on the inner layer and not the outer.

- Selective oxidation due to curvature. As mentioned earlier Kao et al. showed that the curvature of a silicon substrate influences its oxidation rate. This may also be at play in our case.

My objective is to investigate this phenomena and attempt to determine the source of this excess oxygen. The validity of some of these hypotheses will be shown with simple diffusion models. These models will give us a reference to which we may compare our data. The samples were imaged using a transmission electron microscope (TEM) and elemental analysis was obtained using the scanning transmission electron microscopy (STEM) technique.

1.2 Diffusion

In section 1.1 a few possible mechanisms governed by diffusion were suggested that could explain the oxidation of the innermost SiO_2 layer. These hypotheses are as follows: excess oxygen in the SiO_2 layer; excess oxygen in the aluminum; and penetration of oxygen through the sides of the

ribs. Through looking at diffusion rates of various elemental combinations we can get a feel for what is possible and what is not. We use the diffusion length equation:

$$L = 2\sqrt{Dt} \tag{1.1}$$

with L being the diffusion length in cm, D being the diffusivity in cm^2/s, and t being time in sec. The value of L is what we will compare to our rib dimensions to decide which hypotheses are reasonable. The diffusivity D of a crystalline solid is described by the Arrhenius relation:

$$D = D_o \exp(\frac{-Q}{kT}), \tag{1.2}$$

with D_o being the frequency factor or pre-exponential factor in cm^2/s, Q being the activation energy (enthalpy) in eV (D_o and Q are determined experimentally), k being the Boltzmann constant in eV/K, and T being the Temperature in K. Even though this equation is for crystalline materials it is shown by Landolt-Bornstine that this equation may extend to amorphous materials as well (Hsieh & Jain 2012). The values D_o and Q can be found in the literature and sometimes D can be found for a specific range of T.

Evaluation of the diffusion data must be relative to the dimensions of the ribs. The ribs are spaced $\sim$ 100 nm; the layered SiO_2 , Si and SiO_2 measure about 10 nm, 15 nm, 10 nm tall respectively; and the head is $\sim$ 60 nm at its widest.

In table 1.1 we present the diffusion lengths of important elements in our system at 300°, or valid temperatures when a non temperature dependent D was given, and two different times (30 and 60 min). We do recognize that the temperatures used may not be in the range of temperatures for the diffusion data but these were the closest found in the literature for our range of interest. Also the numbers used are bulk diffusion numbers which can be much lower than interface diffusion numbers. These numbers are used to give a ballpark figure of our diffusion lengths.

From table 1.1 the different lengths for H_2O and O_2 diffusion are over 250nm in SiO_2 in 30

Table 1.1 Extrapolated diffusion lengths for elements for *t*=60min and *t*=30min.

Elements	$O_2 \rightarrow Si$	$H_2O \rightarrow SiO_2$	$O_2 \rightarrow SiO_2$
Q (ev)	—	7.96e-1 [2]	1.01 [3]
D_o (cm^2/s)	—	1e-6 [2]	6.7e-5 [3]
D (cm^2/s) (T=300°C)	—	1e-13	8.81e-14
D (cm^2/s) (T= Valid Temp)	5.4e-22 [1]	—	—
L (nm) (t=30min)	0.020	269	252
L (nm) (t=60min)	0.028	380	356
Valid Temp (^{o}C)	$\sim$ 400	600 - 1200	800 - 1200

[1] (J. C. Mikkelsen 1982)

[2] (Hsieh & Jain 2012)

[3] (Kajihara et al. 2011)

min at 300°C. That is more than 4 times the width of the entire rib. Now it is recognized that this length is not calculated using a diffusivity specified at 300°C but has been extrapolated to this temperature. However, even if these numbers were quartered this shows that there would still be plenty of O present for Si oxidation.

The diffusion length of oxygen in to silicon, as seen in table 1.1, is very small. The temperature for which these number given is 400°C. This is much closer to our baking conditions. However, in 60 min at 400°C the O would diffuse only 0.2 Å. This shows that direct diffusion through the bulk of the match head from atmosphere is not a reasonable possibility.

1.2.1 Discussion

At the end of section 1.1 was listed hypotheses for O transport to the inner layer and reasons for the selective growth of that layer. These were:

For transport:

1. Excess oxygen in the inner oxide layer.

2. Free oxygen in the aluminum.

3. O migration up the Si-SiO$_2$ or Al-SiO$_2$ interface.

4. Atmospheric O diffusing through the SiO$_2$ and Si rich layers.

For selective growth:

1. Al$_2$O$_3$ catalysis.

2. Selective oxidation due to curvature.

Looking at these hypotheses we can now rule out some possibilities.

In the transport category hypothesis number 1 is not reasonable since the height of the first (closest to Al) O peaks in the baked and unbaked samples(as seen in figures 1.5 and 1.6) were the same. If this hypothesis was a possibility we would have expected the baked O peak to have a similar under curve area. Thus if the O peak of the baked sample is longer, as observed in figures 1.5 and 1.6, it should also be shorter with respect to the unbaked O peak.

Transport hypothesis number 2 is unreasonable. Integration of the first O peaks shows almost 3x discrepancy between the baked and unbaked samples. Simple calculations show that for all the O needed to produce this growth to originate in the rib it would be composed of Alumina instead of Aluminum.

Transport hypothesis 3 is a real possibility since the diffusion numbers indicate quick transport through bulk SiO_2 . Interface/boundary transport is even faster than bulk thus making this very likely.

Transport hypothesis 4 is not a possibility. Looking at table 1.1 we see that the diffusion of O through Si is very slow and therefore not the mechanism.

Growth hypothesis 1 will be explored by experimentation.

Growth hypothesis 2 is not likely. Kao's paper states that the higher the curvature the slower the oxidation. This would indicate that the inner surface with higher curvature should have slower growth than the outer lower curvature which was not observed.

After reviewing the previous facts our hypotheses are thus: Transport:

- O migration through the SiO_2 or the Si-SiO_2 or Al-SiO_2 interface.

For selective growth:

- Al_2O_3 catalysis.

Chapter 2

Experimental Plan

In section 1.2.1 we listed hypotheses for the growth observed in figure 1.5. In attempting to determine the source of the excess O various adaptations to the rib were made to try to rule out or support the afore mentioned hypotheses. The original rib was Al, coated with SiO_2 followed by a layer of SiX and capped by SiO_2 . These layers were specially engineered by Moxtek for their specific applications. Adaptations to this original rib were as follows:

- Al rib with a SiO_2 - Si - SiO_2 stack

- Al rib with a Al_2O_3 - SiO_2 - Si stack

- AlCu rib with a SiO_2 - Si stack

- Al rib with a SiO_2 - Si and overgrown SiO_2 stack (very thick and bridges the ribs)

The SiO_2 - Si - SiO_2 stack was to discover whether the growth was due to the presence of X in the original structure or if this was a geometric phenomena.

The Al_2O_3 - SiO_2 - Si stack was for two purposes: first to see if the presence of an alumina boundary between the rib and the SiO_2 prevented diffusion between the two; and second to look for evidence of the Al_2O_3 acting as a catalyst for the Si oxidation.

16

The AlCu rib with a SiO_2 - Si stack was done with the idea that if the O was diffusing out of the Al or up the Al - SiO_2 interface then the added Cu would act as a getter for the O.

The SiO_2 - Si and overgrown SiO_2 stack was to isolate the system from the atmosphere, thus preventing the bulk diffusion from the top.

Chapter 3

Methods

3.1   Sample Preparation

3.1.1   Thermal Treatment

To simulate longterm use Moxtek baked the polarizers baked at 300°C for > 100 hrs. They noted that the largest optical change took place in the first 24 hrs. In an effort to better control the experiment some samples were baked at BYU for 24 hrs. These samples baked at BYU are placed in a four inch Lindberg furnace at 300°C. The samples were placed on a quartz boat centered in a quartz tube sealed at both ends thus trapping air inside. After the 24 hours of baking, the furnace is turned off, opened, and allowed to air cool.

3.1.2   FIB

Small sections of the polarizers are broken off to be prepared for microscope analysis. These sections are mounted on a common aluminum SEM stub with colloidal carbon paint. When the paint has dried, these samples are then coated with a layer of carbon between ~ 20 *nm* to ~ 60 *nm* by thermal evaporation. This carbon layer is applied for three reasons: first, to reduce charging of

18
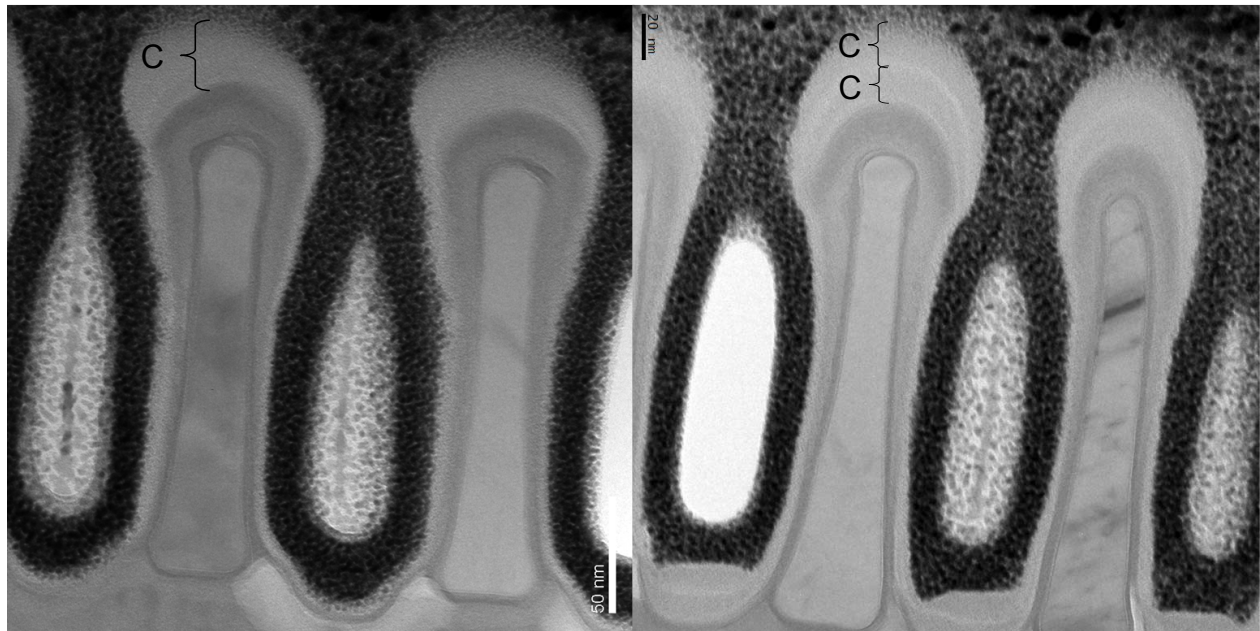
(a) One carbon deposition

(b) Two carbon depositions

Figure 3.1 (a) shows the carbon deposition acquired with the Denton system. (b) shows that with the newer Quorum system the need for 2 cycles results in 2 distinct layers seen in the TEM.

the polarizer sample; second, to protect the absorbing layers of the polarizer from ion damage; and third, to reduce the background x-ray signature at the top of the cap when using Energy Dispersive X-ray (EDX) analysis. The carbon was originally applied with a Denton evaporator and then with a newer Quorum system. Only one coating was needed when using the Denton, however there was no sample rotation thus producing an asymmetric coat (see fig 3.1a). The Quorum, on the other hand ,requires 2 cycles and rotates the sample creating a more symmetric coat (see fig 3.1b). The settings for the pulse rod deposition used for the new system are as follows: Current 70 amps, 3 pulses, 10 s/pulse, with the rotation at 100 rev/min. Running the sample through this process twice creates an additional layer that is visible in the TEM images (see fig 3.1).

Once the samples are coated they are put into the Focused Ion Beam system (FIB). The purpose

Step	Current	Magnification	Time
1	5.4 pA	2000x	1 min
2	1.4 nA	2000x	3 min
3	1.4 nA	3500x	4 min
4	2.7 nA	2000x	3 min
5	2.7 nA	5000x	3 min
6	2.7 nA	2000x	1 min

Table 3.1 Procedure used for e-beam Pt deposition to protect from ion damage. These steps are done in quad screen mode at 0° tilt, beam energy at $5 \ keV$.

of using the FIB is to create a 15 μm long by 5 μm high cross section sample of the polarizer ribs. After aligning the ribs vertically on in the electron beam (e-beam) window, the e-beam is used to create a platinum protection layer. This first Pt layer is laid to protect the sample from the relatively high energies of the ions used to deposit Pt during the automated process. By using low energy electrons to deposit a primary Pt layer we can reduce ion implantation and damage to the surface layers of interest. Table 3.1 is the "recipe" used for the e-beam Pt deposition. This recipe was used to prevent damage from high energy electrons and has been included for completeness in documentation. This recipe is followed while in quad screen mode at 0° tilt beam energy at 5 keV and a dwell time of 300 ns.

After the application of the e-beam Pt, the program Auto-TEM is used to do the cross section cut out. Before running the script the maximum beam current is set to 28 nA in the Auto-TEM settings tab and the program is used to lay an additional grounding pad and to mill the fiducial

marks. After this is done the Auto-TEM script can be run. Upon completion of the script, the sample is labeled, lifted out using the Omniprobe needle, and Pt welded onto the Cu lift out grid. Once the sample is on the grid a three step process is used to thin the sample leaving it $< 100nm$. At this point it is ready for the TEM. This is a standard procedure for cross section TEM sample preparation in the FIB.

3.2 Analysis Methods

3.2.1 Imaging

The TEM system used is a Tecnai TF20 Analytical STEM. When used for this project it is run with a beam energy of 200 keV, with a 70 μm C$_2$ aperture. While in TEM mode a spot size of 5 is used and bright field images are taken with the 20 μm aperture. This spot size was chosen to minimize charging and beam damage. While in STEM mode the spot size is increased to 7 to maximize the x-ray count. Images in TEM mode are taken at 2500x , creating a mosaic of the whole sample. Then at 38 kx, a mass thickness image (no aperture) and a bright field image are taken of the same location. Finally at 66 kx both mass thickness and bright field images are taken of the same location. In STEM mode an additional image is acquired at 580 kx.

3.2.2 STEM

In Scanning Transmission Electron Microscopy (STEM) the electron beam is focused to a fine point or probe. This probe is then rastered across the sample much like how the old CRT monitors functioned. As the beam is scanning, a detector collects the information at each spot and feeds it to the computer creating an image.

Also in STEM mode one can create a path (shown in figure 3.2(a)) for the probe to follow, stopping at given intervals for a given time. For our path scans we use 150 data points with a

beam dwell time of 3000 ms with drift correction. These paths were usually 75 nm long. As the electrons interact with the atoms in the sample, x-rays are scattered that are unique to the elements with which the electrons interacted. These x-rays are collected and produce spectra indicating which elements are present at a given point (see figure 3.2(c)). This process is called Energy Dispersive X-ray Spectroscopy (EDXS or EDS). Once a spectrum is collected for each point in the path, the data can be extracted for a given energy window to create an elemental signal vs distance graph (see figure 3.2(b)). The energy windows used were each 0.1 keV wide and centered around 0.2770 keV (carbon), 0.5230 keV (oxygen), 1.486 keV (aluminum), and 1.740 keV (silicon). The graph provides an elemental profile along the path that was selected. This line is scanned in one direction and rescanned in the opposite direction to check reproducibility of the scans.

3.2.3   Data Processing

Once the elemental profiles are acquired, the raw data is exported to Excel. The data is normalized to the highest Al count. No horizontal scaling is done in order to preserve position confidence. The scan and rescan are overlaid and the Al edges are aligned. To reduce noise in the signal some data has been averaged using three or five point averaging. This averaging can cause a 1.5 nm or 2.5 nm smearing for the three and five point averaging respectively. If there are baked and unbaked samples their profiles are overlaid to look for differences in shape.
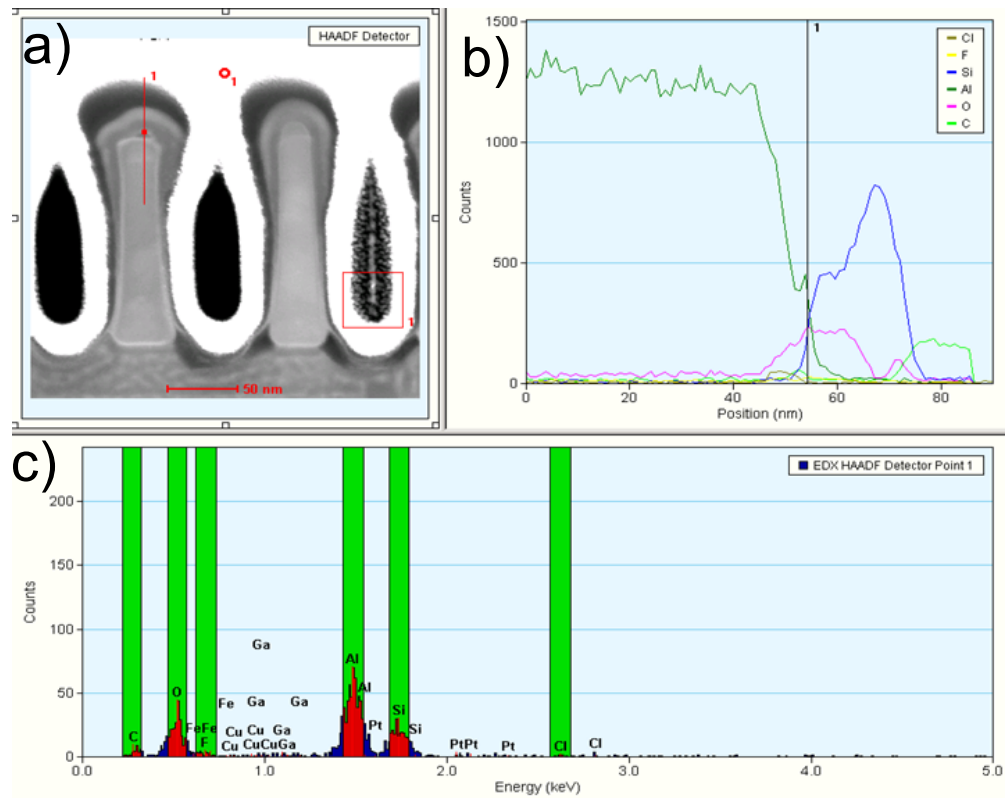
Figure 3.2 This is a typical data view. Window a) is the STEM image of the rib to be analyzed. The line on the first rib was path taken by the probe. b) shows the profile of the various elements highlighted in c). c) is the xray spectrum for a given point on the path shown in figure a).

Chapter 4

Modeling

4.1 Tilt

During the mounting process described in section 3.1.2 the sample may be welded at some nonzero angle with respect to the grid. It is thought that this angle could affect the profiles obtained in STEM mode since the electrons would no longer be interacting with the sample perpendicularly but at some angle from perpendicular. It is assumed that this angle would cause a smearing of the elements of the trace. In order to find out if this issue needs to be addressed some simple calculations were done. We first define the variables d, d', t, θ, θ', and k as defined in figure 4.4. This figure models a layer (blue) sandwiched between two other layers (red). The variable d is the actual width of the blue layer; t is the sample thickness, determined by FIB thinning process. For an arbitrary nonzero tilt of θ there are overlap regions in the projection (purple regions in fig. 4.1b). The length of these regions are represented by k and the remaining blue region is given by d'. If θ gets large enough the blue region disappears, $d' = 0$. This angle will be referred to as the critical angle θ'.

It is necessary to know what this critical angle is for a given width and thickness. By looking

24

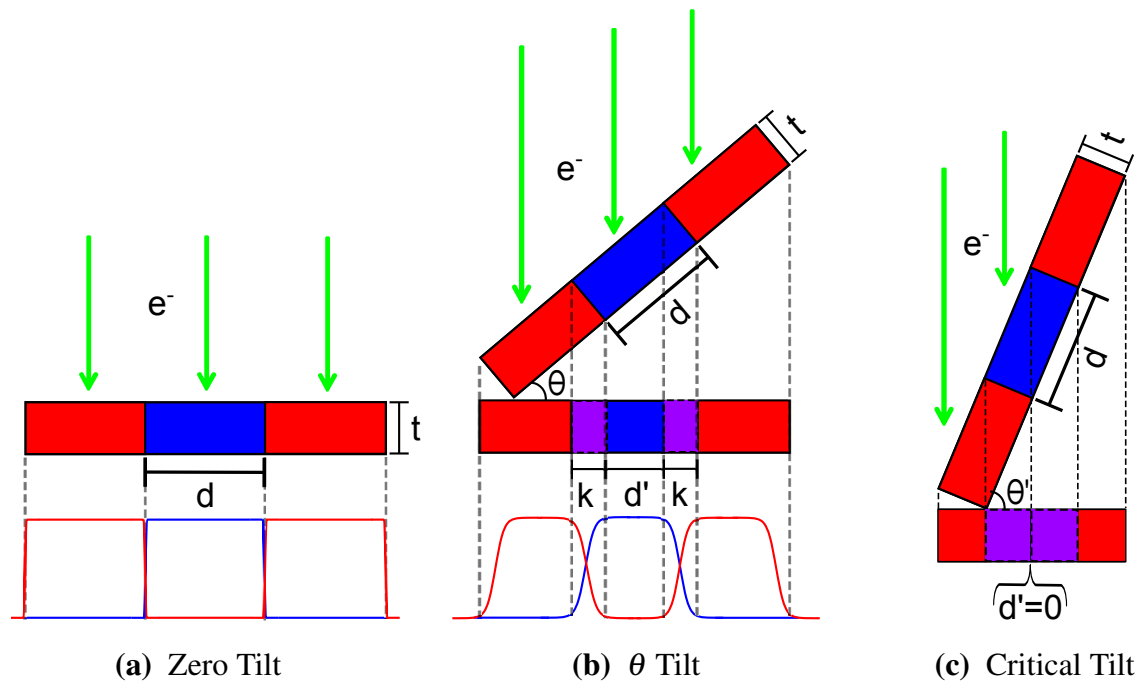**(a)** Zero Tilt   **(b)** θ Tilt   **(c)** Critical Tilt

Figure 4.1 Various degrees of tilt. Figure (a) represents what we expect with zero degree tilt, perpendicular to the electron beam. Figure (b) represents some arbitrary nonzero tilt of θ. Figure (c) displays a critical tilt (θ') condition where there is no blue region in the projection.

at figure 4.1b we can make a right triangle with d as the hypotenuse and the length $d' + k$ as the base. Recalling the definition of cosine we get

$$cos(\theta) = (d' + k)/d. \tag{4.1}$$

Since k is the length of the projection of the overlapping region we can express it as

$$k = t * sin(\theta). \tag{4.2}$$

Combining these two equations and solving for d' we get

$$d' = d * cos(\theta) - t * sin(\theta). \tag{4.3}$$

If we wish to find the critical angle θ' at which $d' = 0$ then we get

$$\theta' = arctan(d/t). \tag{4.4}$$

Now if by inserting reasonable numbers for d and t we can know if layers could disappear due to tilt. Using 10 nm for d and 100 nm for t we find that $\theta' = 5.7^o$. So about $+/-6^o$ is the margin we need to be with in.

Figures 4.2 and 4.3 show experimentally the results of tilting the sample. In figure 4.2 each elemental profile was taken at 1 degree increments starting with 1° and ending with 5°. This range was chosen since the above calculation predicted the critical angle to be $\sim 6^o$. However, as you can see in the figure all of the major features of the scans match up. This matching indicates that the critical angle was not reached, therefore our sample must be much thinner than 100 nm.

Because the critical angle was not observed in figure 4.2, data was taken from the same sample at 0, 5, and 10 degrees. This data is shown in figure 4.3. This data was overlaid and aligned using the middle of the Si peak. It can be clearly seen that the Si peaks of the 0 and 5 degree scans match.
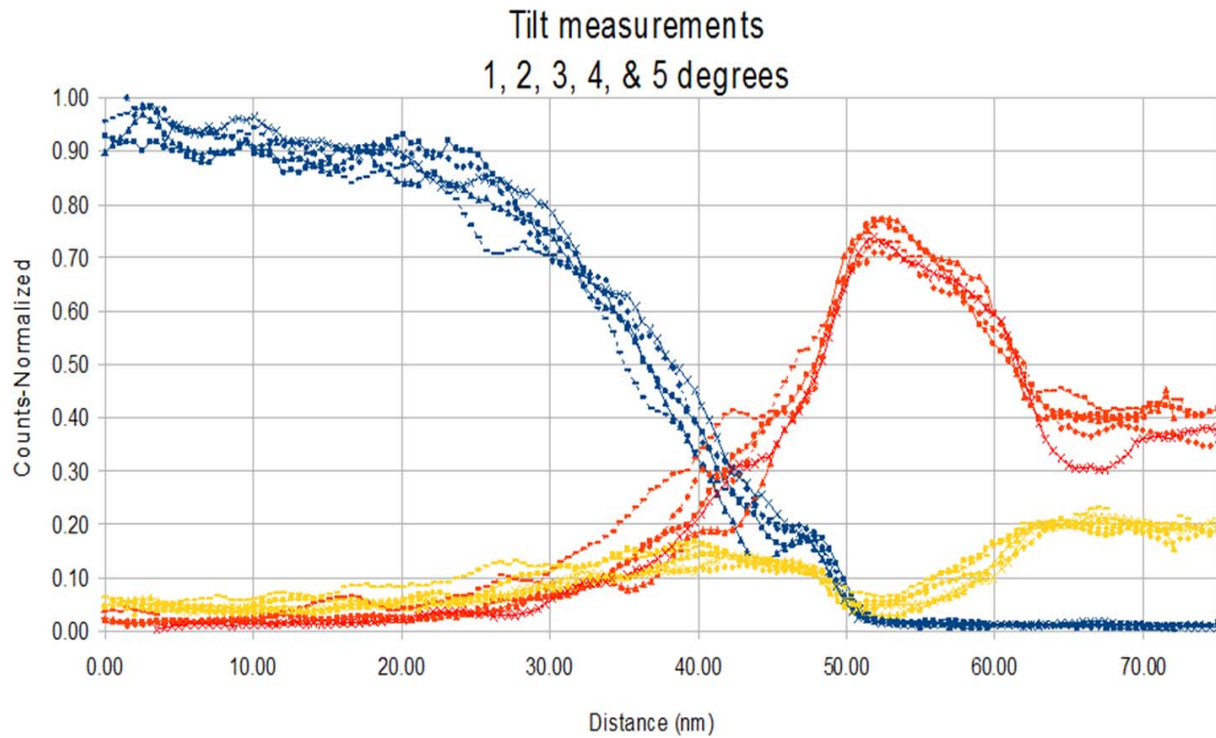
Figure 4.2 Data taken from one rib at 1, 2, 3, 4, and 5°. This data was taken to observe the approach to the theoretical 6° critical angle(θ'). As is plain to see these scans all matched up quite nicely showing that $\theta' > 6^o$; consequentially showing that the $t << 100$ nm and the effects of sample tilt are not significant.
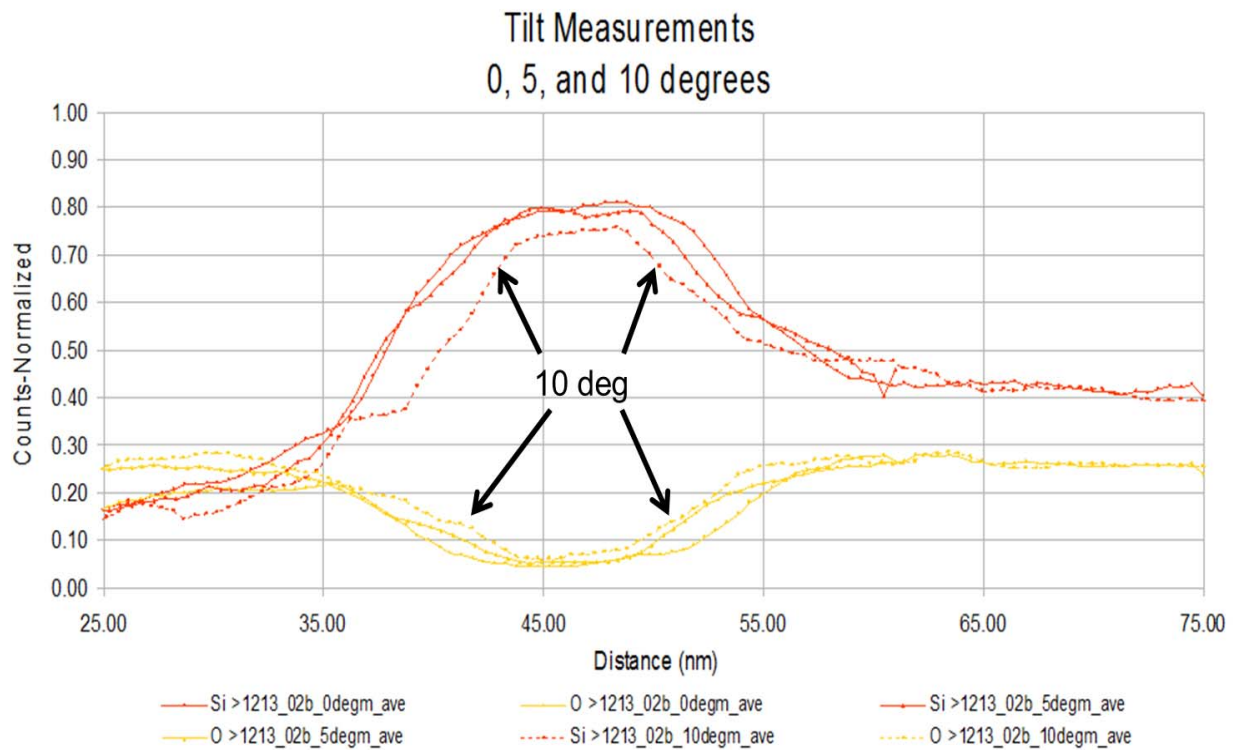
Figure 4.3 Data taken from one rib at 0, 5, and 10°. Here we can see at 10° that sample tilt begins to affect the Si peak.

This is in good agreement from what we found in the first experiment tilting from 1 to 5 degrees. However, the 10 degree scan is considerably thinner than those of the 1 and 5 degree scans. This indicates that somewhere between 5 and 10 degrees the angle begins to have a visible affect on the scans. The mounting angle of the samples never exceeded $\sim 5^o$ and therefore the tilt of the sample is not significant.

4.2 Probe Shape

Just as the tilt, as discussed previously, can blur the interface, so can the shape of the STEM probe described in section 3.2.2. Data was taken to help create a one dimensional model by scanning perpendicularly across a sharp boundary (vacuum to Si) and and recording the counts on the HAADF detector. Three such paths were then averaged and used as the data to be fit. Figure 4.4a shows the initial conditions to the model. The blue shelf represents the sharp edge and the green Gaussian the probe. These two shapes were convolved to model the signal expected from a certain probe shape. The probe shape was manipulated, changing the center and the σ, to best fit the data. Figure 4.4b shows the convolution (green) fit to the data (blue). Once a good fit was obtained the FWHM of the probe was calculated using the σ value. In this case, as noted on figure 4.4b we see the FWHM is almost 5 nm. This data was taken using the 70 μm C$_2$ aperture. This process was followed using the 150 μm aperture as well and the Al data from one of the rib scans. The 5 and 4 nm values were wider than expected. These values can be effected by defocus values, and variance in the samples themselves.

As can be seen in table 4.1 the calculated FWHM of the Al scan was much bigger than either of the other two scans. This indicates that the Al boundary is not sharp. Or in other words there is some mixing of elements at the Al surface.
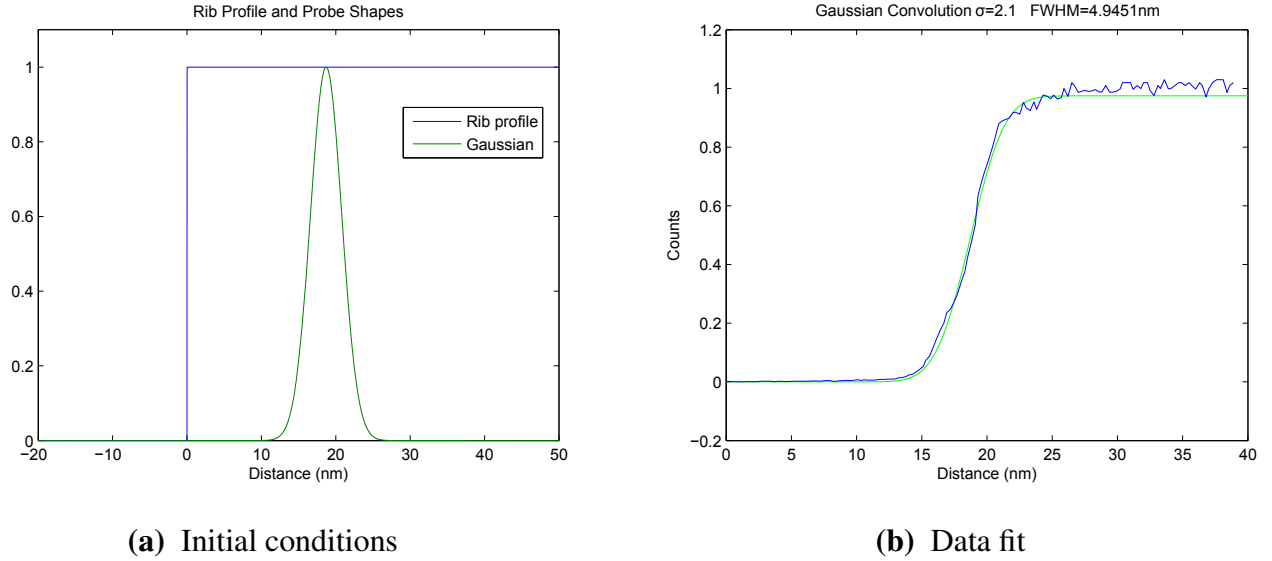
(a) Initial conditions

(b) Data fit

Figure 4.4 The initial conditions of the model are shown in (a). These being a step function representing the sharp boundary and the Gaussian representing the probe shape. The convolution of the shapes in (a) (green) are fit to the data in panel (b) (blue).

Data Profile	Probe FWHM
70	4.95 nm
150	4.00 nm
Al	7.06 nm

Table 4.1 The calculated FWHM of the Gaussian probe whose convolution with a step function best fits the data.

Chapter 5

Results

As mentioned in section 3.2.3, the data acquired from the elemental scans is put into excel and are aligned and averaged in preparation for comparison. Twenty-four samples were processed as before and after sets. Here we show the data collected on the sample labeled 1150_02-B2 as an example of the analysis process. The results of the remaining samples are summarized in table 5.1 with some notes on interesting samples in the appendix.

The sample 1150_02-B2 is expected to have a SiO_2 layer followed by a Si layer with no capping layer. The unbaked sample will be referred to by 1150_02-B2 and the baked by 1150_02b-B2. The original sample was broken in half, one half being baked at BYU as described in section 3.1.1, the other half was used as the control. Figure 5.1 shows mass thickness contrast images of these unbaked and baked samples.

In figure 5.2 we see the elemental profile for the unbaked 1150_02-B2 sample. The Al profiles have been properly overlaid to allow comparison of the unbaked and baked samples. The first thing to note is that the two traces of this vertical scan seem to be in good agreement; meaning all of the major features of the first trace are mimicked in the retrace. Note the two peaks in the O counts, one large peak and the a small bump just inside the Si on the right of the picture. The first, closest to the Al, is the deposited SiO_2 and the second is the native oxide formed due to exposed Si. These

31
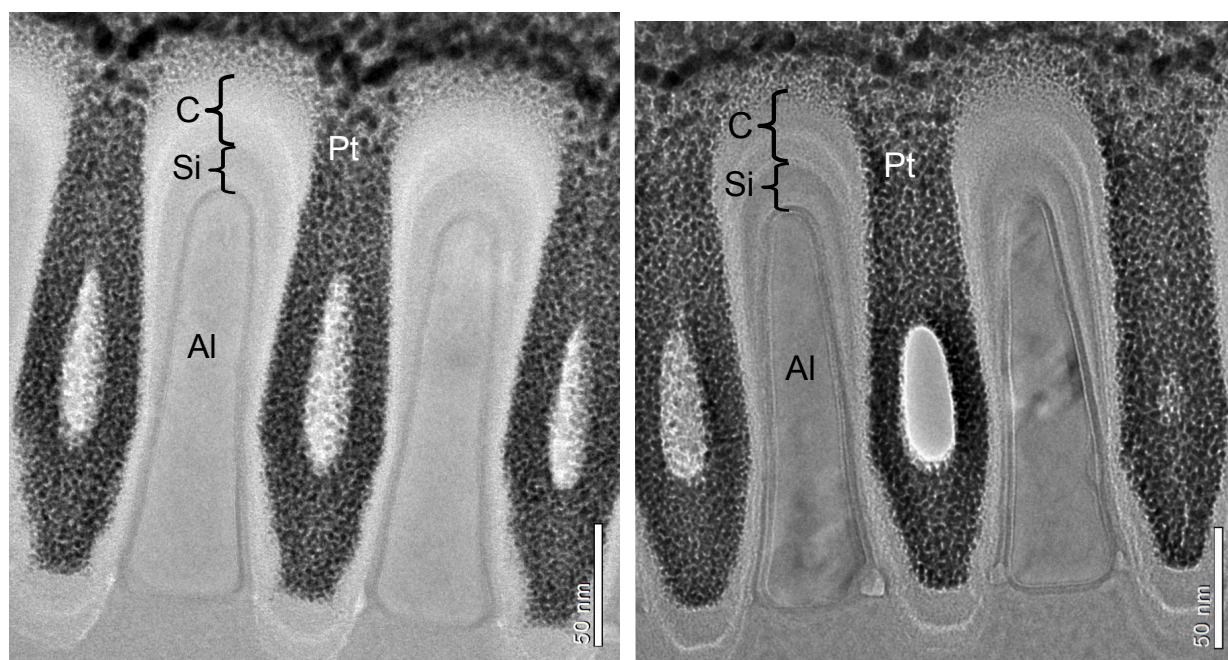
(a) Unbaked sample 1150_02-B2   **(b)** Baked sample 1150_02b-B2

Figure 5.1 Here are side by side images of sample 1150_02-B2, Al rib with a SiO_2 - Si stack, before and after baking. The major elemental regions are labeled. The portion labeled as Si refers to the Si layers, SiO_2 - Si.
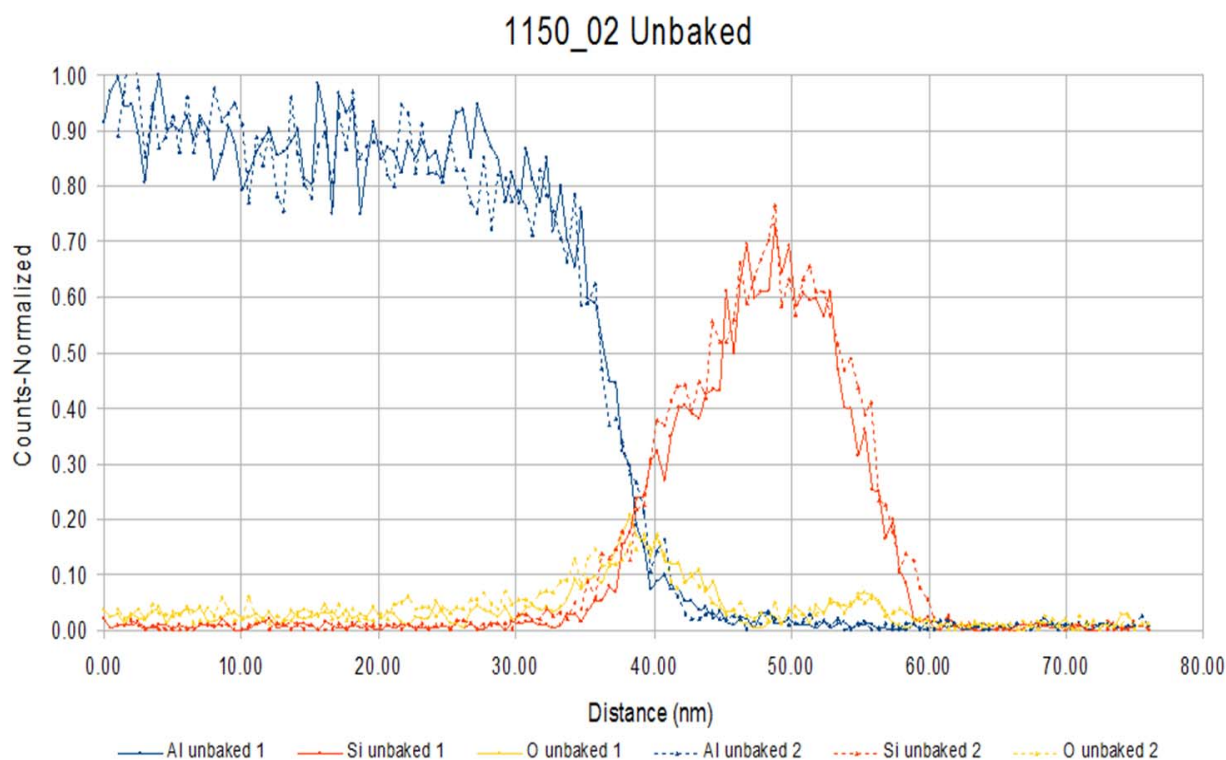
Figure 5.2 This is the elemental profile of the unbaked sample 1150_02.

features are to be expected from what we knew of the layer composition. Along with that we see a slight shoulder in the Si counts just above the O which is a common marker of the SiO_2 layer.

There do exist some peculiarities however. looking at the O counts just under the Al drop off we see the O counts pick up before the Si indicating possible O in the Al at the top of the rib. Also, there is not a strong O peak on the outside indicating a SiO_2 cap but there is the small O peak, mentioned earlier, indicating the native oxide formed after production. However, this peak is deeper in the Si than would be expected. It would be anticipated that it would be just inside the Si decay and drop to zero with the Si. Instead we see it dropping of a little bit earlier.

Figure 5.3 is the elemental profile of the baked 1150_02b-B2. Again we see good correlation
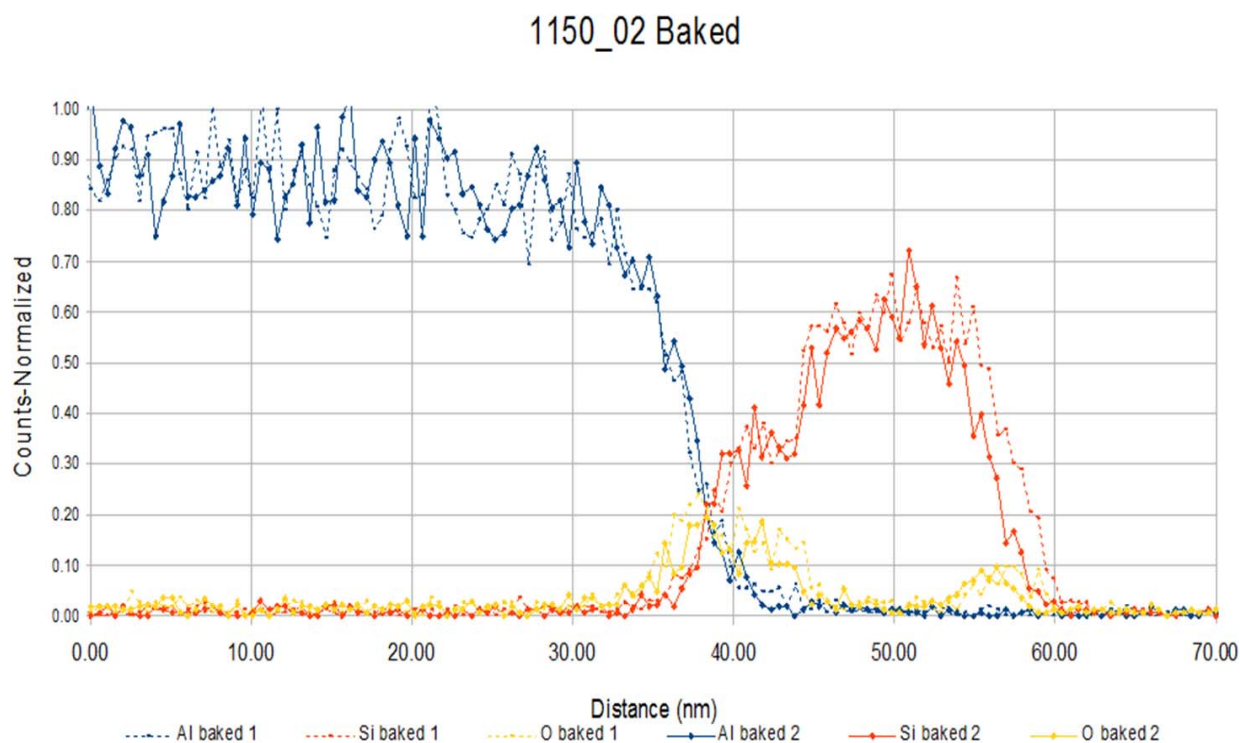
Figure 5.3 This is the elemental profile of the baked sample 1150_02b.

between the scan and rescan profiles. There is some deviation of the Si and O on the right side of the graph. This difference is most likely due to path misalignment as described in section 1.1. The main features do still show up and are mimicked in each scan such as the 2 O peaks and the unique shape of the Si peak. Again we see the O picking up before the Si indicating a possible Alumina layer. This was seen in the unbaked sample but not as strong as this sample. Also, the plateau that was barely visible in the unbaked sample is now clearly visible and we can see a correlation between the O peak and the Si plateau. The outside O peak seems to be stronger in this sample than the other as well. This is to be expected since this sample was baked in atmosphere giving it plenty of time to capture more O in that outer native oxide layer.

Now in figure 5.4 we have overlaid the data from figures 5.2 and 5.3 and averaged over 5 point to reduce noise. The solid lines correspond to the unbaked sample and the dashed to the baked. We first see that the Al profiles lineup nicely giving us confidence in the alignment of these data sets. The width of the Si peak seems to match up nicely except for the wider peak that we discussed in the previous paragraph. Both data sets show non-zero O levels in the Al region near the interface however neither the unbaked or the baked profiles differ greatly than the other. Looking at that first O peak , this is where we would expect to see the expansion seen in the sample in section 1.1. However, as you see here there may be a slight expansion but not large enough to be assured that it is not noise. The second O peak shows stronger O counts for the baked sample than the unbaked for reasons explained earlier. As for the Si peak, we see good agreement save the more pronounced plateau above the first O peak.

The conclusion on this sample is that the evidence for oxide expansion is weak. There were observed a few changes in features but the no significant growth was seen.
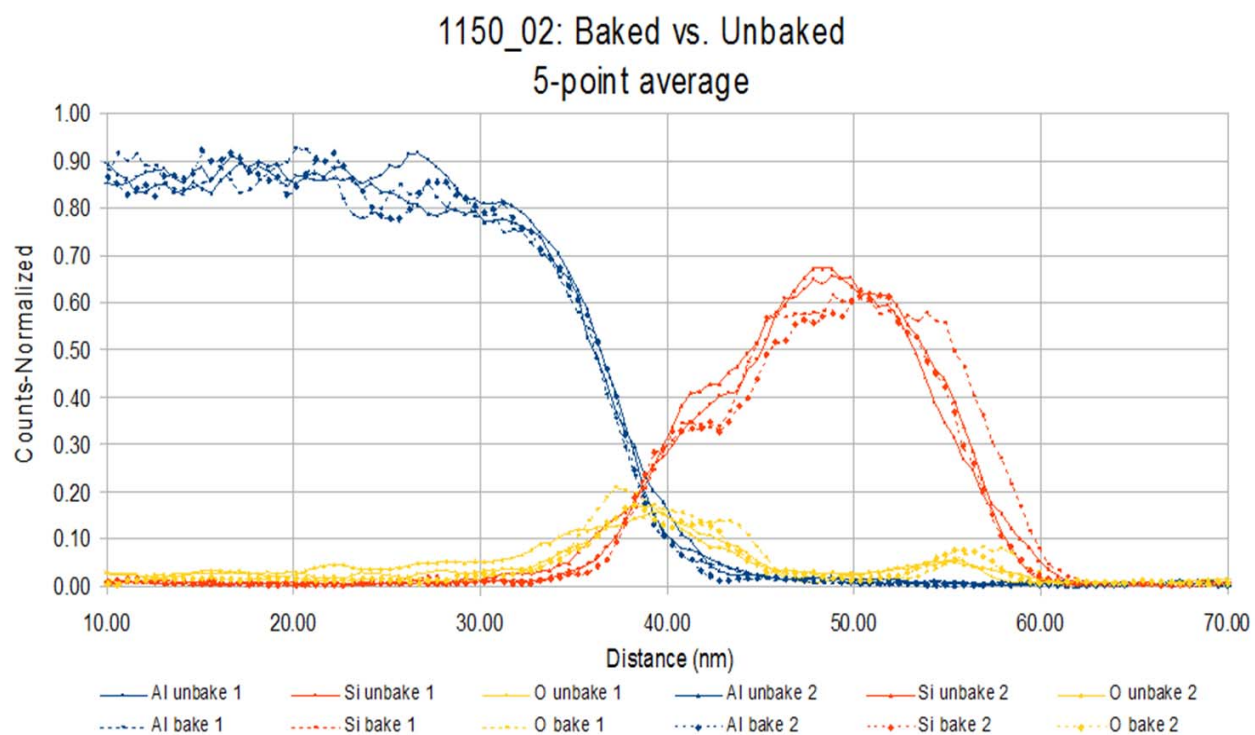
Figure 5.4 This is an overlay of figures 5.2 and 5.3 that has been 5 point averaged to better show difference in features. It can easily be seen here that there was no significant growth of the inner SiO_2 layer after baking.

Table 5.1 Here we present the samples run and the results from our studies. Stared items (*) are discussed further in the appendix.

Series	Name	Features	Baked? By Whom?	Results: Baked vs. Unbaked
1043	01-ID	SiO_2 - SiX - SiO_2	N	- Growth of inside SiO_2 layer observed.
	02-SD		Mox	
1136	01	SiO_2 - Si	N	- There may be some pull of Si into the Al or Al into the Si. - The O peaks seem not effected by the bake save for a seeming higher O back ground in the Al region.
	02		Mox	
	03		N	- The only noticeable difference between these samples is the dip in the first O peak. However, it is uncertain if that was a result of the bake or production.
	04		Mox	
1143	05a	AlO_3 - SiO_2 - Si AlCu Ribs	N	- No clear difference.
	05b		BYU	

Table 5.2 This table is a continuation of table 5.1. Stared (*) items are addressed in the appendix.

Series	Name	Features	Baked? By Whom?	Results: Baked vs. Unbaked
1150	01	SiO_2 - Si - SiO_2 Large Cap	N	- Uncertain due to noise
	01b		BYU	
	02	SiO_2 - Si	N	- The inner O layer does not seem to change. - the outer O layer seems to extend away from the rib.
	02b		BYU	
	03		N	- Inner and outer O peak seems stronger but of similar widths. - No discernible width change.
	03b		BYU	
	04		N	- No discernible change.
	04b		BYU	
	05		N	- No discernible change.
	05b		BYU	
	06		N	- No discernible change.
	06b		BYU	
1213	01a	SiO_2 - Si - SiO_2	N	- Possible expansion of the inner SiO_2 layer ($\sim$ 3-4nm). - Deeper Al penetration in the inner SiO_2 region in the baked sample
	01b		Mox	
	02a	SiO_2 - Si - SiO_2 Large Cap	N	- Possible diffusion of SiO_2 into the Al rib.
	02b		Mox	

Chapter 6

Conclusion

In our study we processed 12 sets of before and after samples making a total of 24 samples not including the original pair. The composition of the layering and the ribs were varied to try to determine the mechanism and source of the O causing the inner SiO_2 layer growth. In an effort to simplify the problem the element X was removed leaving Si middle layer instead of a Si rich SiX layer. The growing effect could not be replicated in any of these sets. The original unbaked sample was baked at BYU and analyzed but no growth was observed. This lack of observation leads to the conclusion the original samples were not comparable to start, that they were not a before and after as indicated.

Appendix A

1136_01 & 02 (SiO$_2$ - Si)

In figure A.1 the graph is aligned at the bottom of the Al curve of both the baked (01) and unbaked (02). The Al curves do not have the same general curvature. The choice to align the bottom of the curve was made since it lined up the outer silicon traces. However, if the shoulder of the Al were to be aligned the inner Si traces would be in more agreement. This poses the question if the Si is being pulled into the Al or the Al into the Si.

As far as the O profiles go there are higher O counts in the Si for the baked sample than the unbaked with the current alignment. Once the O traces enter the Si region they appear relatively unchanged.

Conclusion:

- There may be some pull of Si into the Al or Al into the Si.

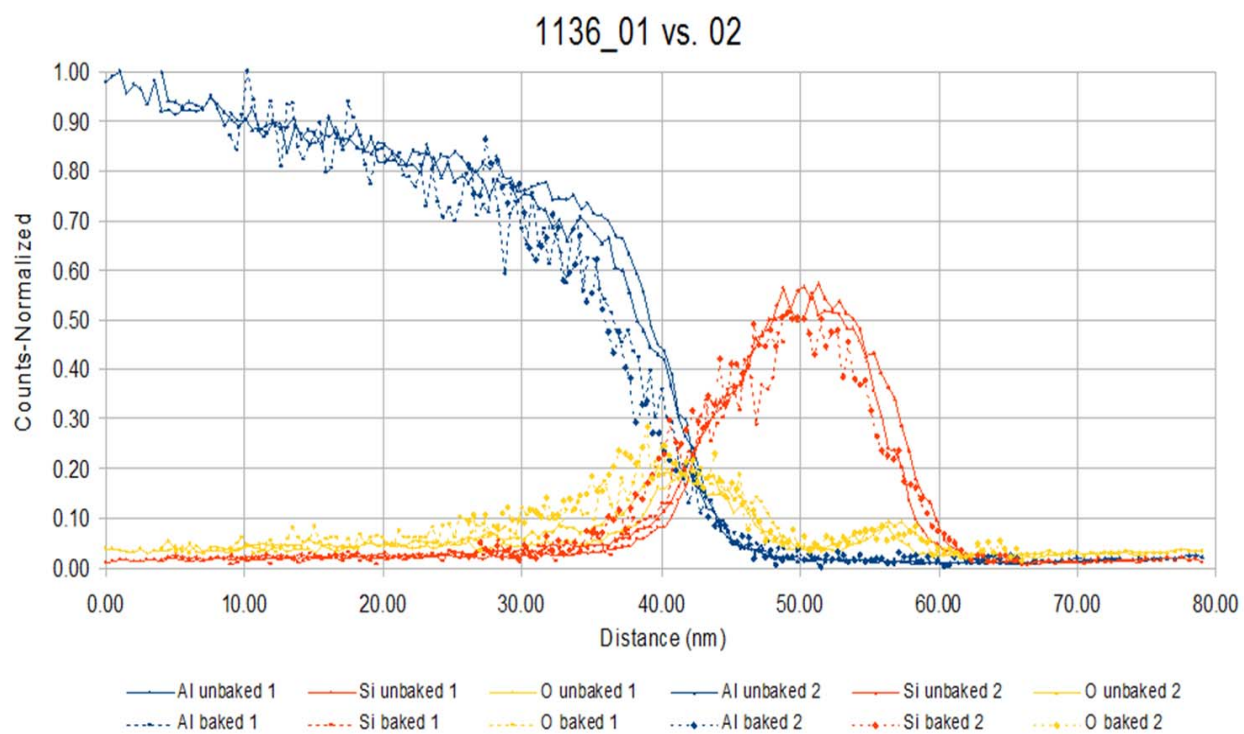- The O peaks seem not effected by the bake save for higher O counts in the Al region.

Figure A.1 Unbaked vs. baked 1136_01 and 02 samples. Al profiles have been aligned using the bottom of the curve instead of the shoulder.

Appendix B

1213_01a & 01b (SiO$_2$ - Si - SiO$_2$)

In figure B.1, all features seem to more or less align. The only exception being the Al counts of the 01b sample penetrate deeper in to the inner O peak. This may be an indication of diffusion of the Al into the SiO$_2$.

Upon close inspection of the inner O peak, it can be seen that the baked sample O peaks extend 3-4 nm further than that of the unbaked.

CONCLUSION:

- Possible expansion of the inner Sio2 layer (3-4nm).

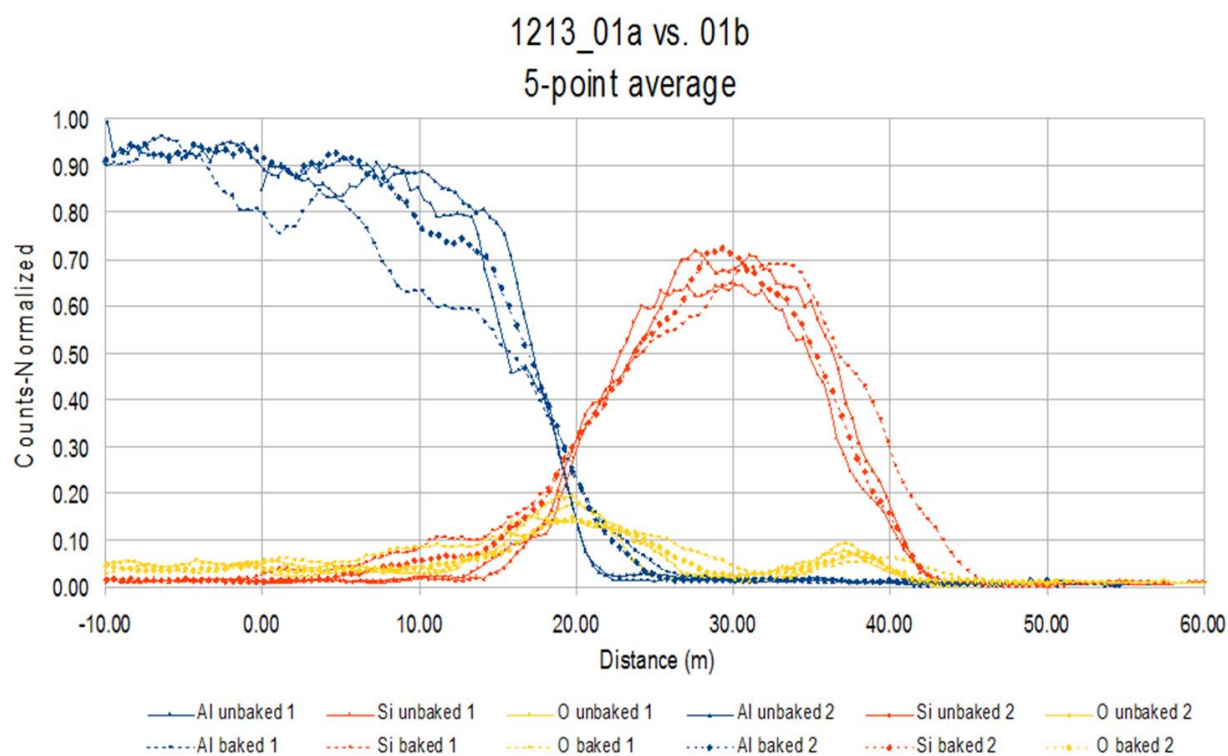- Deeper Al penetration in the inner SiO2 region in the baked sample.

Figure B.1 Unbaked vs. baked 1213_01 and 01b samples. Baked Al penetrates deeper into the O peak.

Appendix C

1213_02a & 02b (SiO$_2$ - Si - SiO$_2$ overgrowth)

Looking at the first O peak in figure C.1, it can be seen that the baked O and Si counts just before the interface are greater than those of the unbaked. However, there does not appear to be any expansion of the SiO$_2$ layer into Si region to indicate SiO$_2$ growth. Also, the Al peak extends farther into the Si peak than previously seen.
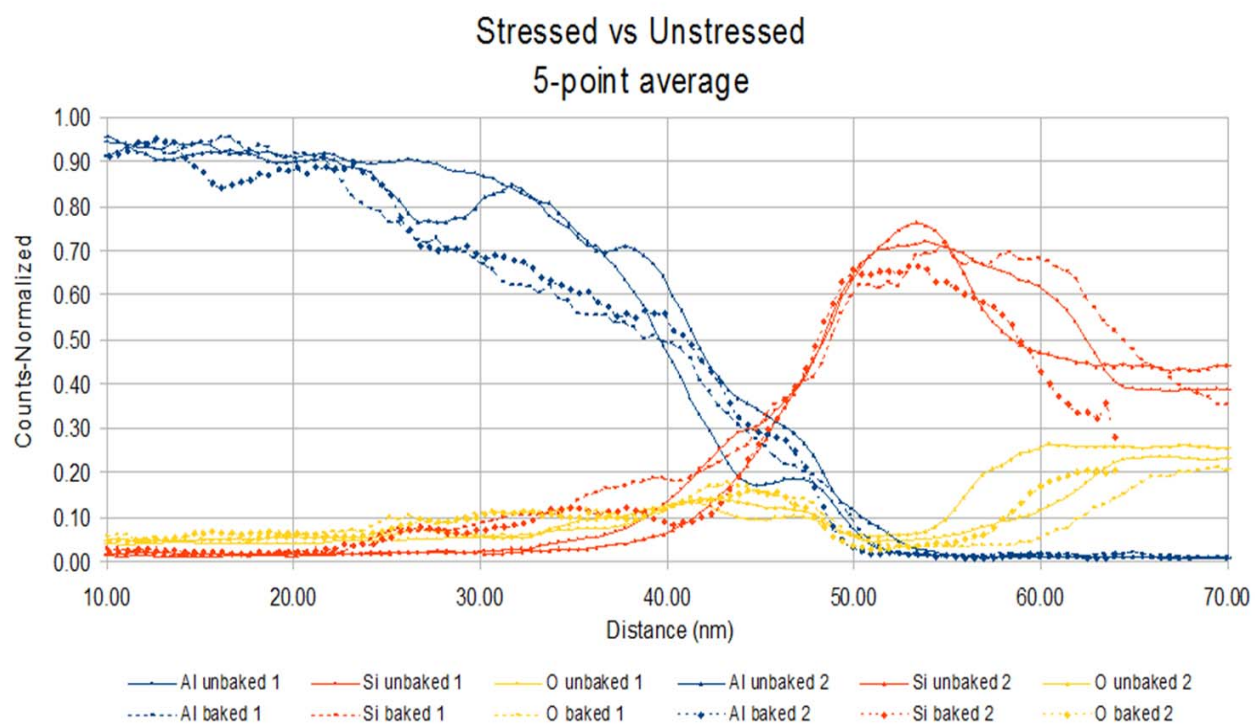
Figure C.1 Unbaked vs. baked 1213_02 and 02b samples. Baked Al penetrates deep into the Si region.

Bibliography

Akermark, T. 2000, Journal of The Electrochemical Society, 147, 1882

Bongiorno, A., & Pasquarello, A. 2002, Phys. Rev. Lett., 88, 125901

Deal, B. E., & Grove, A. S. 1965, Journal of Applied Physics, 36, 3770

Gusev, E. P., Lu, H. C., Gustafsson, T., & Garfunkel, E. 1995, Phys. Rev. B, 52, 1759

Hamann, D. R. 1998, Phys. Rev. Lett., 81, 3447

Hsieh, C. H., & Jain, H. 2012, SpringerMaterials - The Landolt-Bï£¡rnstein Database, 33B1: Diffusion in Non-Metallic Solids (Part 1)

J. C. Mikkelsen, J. 1982, Applied Physics Letters, 40, 336

Kajihara, K., Miura, T., Kamioka, H., Hirano, M., Skuja, L., & Hosono, H. 2011, Phys. Rev. B, 83, 064202

Kao, D.-B., McVittie, J., Nix, W., & Saraswat, K. 1987, Electron Devices, IEEE Transactions on, 34, 1008

Lu, H. C., Gustafsson, T., Gusev, E. P., & Garfunkel, E. 1995, Applied Physics Letters, 67, 1742

Zhong, C., Jiang, Y., Gong, J., Deng, B., & Li, J. 2009, Applied Physics A: Materials Science and Processing, 97, 671, 10.1007/s00339-009-5286-z

46